Observations of a torus in a model of the Belousov–Zhabotinskii reaction

Dwight Barkley, John Ringland, and Jack S. Turner
Center for Studies in Statistical Mechanics and Department of Physics, The University of Texas at Austin, Austin, Texas 78712

(Received 1 May 1987; accepted 23 June 1987)

The first observation of quasiperiodic oscillations in a model of the Belousov–Zhabotinskii reaction is presented and the evolution along two parameter paths of the associated torus is described. Comparison is made with experiment and the hysteresis–Hopf normal form. The model dynamics is shown to be more complex than that of the normal form. The torus is also shown to be related to two other features of the BZ reaction: (1) the transition from small amplitude to mixed-mode oscillations and (2) alternating periodic–chaotic sequences.

I. INTRODUCTION

It is well known that in a continuous flow reactor many chemical reactions can exhibit sustained temporal oscillations. Studies of the Belousov–Zhabotinskii reaction in well-stirred flow reactors have revealed much more than simple periodic oscillations; a rich variety of more complex dynamical behavior has been found both in experiments and in simulations.[1–10] Among the more interesting and important experimental observations is that of quasiperiodic oscillations.[11–13] Such oscillations are generally described as containing two incommensurate frequency components (two peaks in the power spectrum at frequencies whose quotient is irrational). More precisely, such oscillations correspond to trajectories in the state space of the system which wrap densely on the surface of a torus.

The existence of quasiperiodic oscillations in the BZ system is important for the following reason. It has been shown[14,15] that quasiperiodicity can result from nonlinear interaction between two elementary bifurcations in the BZ system: the Hopf and the hysteresis bifurcations. It is also known that quasiperiodicity often gives rise to other complex behavior, e.g., chaos, in nonlinear systems.[16–21] Thus it has been suggested that the interaction of the Hopf and hysteresis bifurcations may account for much of the complex dynamics seen in the BZ reaction and that a mathematical model of this interaction, the hysteresis-Hopf normal form, may provide a comprehensive description of this dynamics.[22,23]

Until now, quasiperiodicity has not been observed in a model of a chemical reaction (excluding the case of coupled oscillators[24]) and it has not been possible to compare model results with experiment and the hysteresis–Hopf normal form. In this paper we describe the occurrence of quasiperiodicity in an Oregonator model[25] of the Belousov–Zhabotinskii reaction and show how the torus associated with these quasiperiodic oscillations evolves as parameters in the model are varied. We compare our results with experiment. We show that despite a strong similarity between the evolution of the torus in the model and the evolution of a torus in the hysteresis–Hopf normal form, the model behavior is more complex than can be accounted for with the normal form.

We show that tori, apart from being of importance in the normal form approach to the dynamics of the BZ reaction, can be associated with other complex dynamics seen in the reaction. In particular, the torus we have observed is associated with (1) a transition from a state of nearly harmonic oscillations, to a state consisting of a mixture of nearly harmonic and relaxation oscillations,[1] and (2) a periodic–chaotic sequence: a sequence of states in which the character of oscillations alternates between periodic and chaotic as a control parameter is varied.[2]

II. THE MODEL

The model which we have used in our study is a modified Oregonator proposed by Showalter, Noyes, and Bar-Eli (SNB).[25] It consists of the following six reaction steps:

$$A + Y \underset{k_{-1}}{\overset{k_1}{\rightleftharpoons}} X + P,$$

$$X + Y \underset{k_{-2}}{\overset{k_2}{\rightleftharpoons}} 2P,$$

$$A + X \underset{k_{-3}}{\overset{k_3}{\rightleftharpoons}} 2W,$$

$$C + W \underset{k_{-4}}{\overset{k_4}{\rightleftharpoons}} X + Z,$$

$$2X \underset{k_{-5}}{\overset{k_5}{\rightleftharpoons}} A + P,$$

$$Z \xrightarrow{k_6} gY + C,$$

where $A \equiv BrO_3^-$, $Y \equiv Br^-$, $X \equiv HBrO_2$, $P \equiv HOBr$, $W \equiv BrO_2\cdot$, $Z \equiv Ce^{4+}$, $C \equiv Ce^{3+}$. (Note that we shall use these same capital letters to denote the concentrations of the corresponding chemical species; the meaning will be clear from the context.) This kinetic scheme gives rise in the usual way to a system of coupled ordinary differential equations for the concentrations of the chemical species in a flow reactor.

We note that standard methods[26,27] allow the identification of two stoichiometric constraints for this kinetic scheme. In particular the following two quantities are conserved:

$$C + Z,$$

$$(1 + 6g)A + (1 + 2g)P + (1 + 5g)W + (1 + 4g)X + Y + gZ,$$

where here capital letters denote concentrations. The first

 0021-9606/87/193812-09$02.10

constraint is evident from the kinetic scheme and represents the conservation of cerium; the second expresses a more obscure conservation for the model. As a result of these constraints we can express the concentrations of two of the chemical species as a function of the other five. We choose P, W, X, Y, and Z as the five dynamical variables.

The values of the rate constants appearing in this model have been the subject of considerable controversy.[28–31] While consensus is developing for rate constants in the vicinity of the Tyson "*Lo*" set, the use of these constants in the SNB model may not result in the best agreement with experiment[32] (see also Ref. 29). It is known, however, that with the rate constants given originally by Field, Körös, and Noyes[33] and Field,[34] this and similar models give dynamics qualitatively similar to that found experimentally.[5,9,23,35,36] Because our focus is on the qualitative dynamics of the reaction, we use the values originally given for the rate constants $k_1, k_{-1}, \ldots, k_{-5}$ of the first five reactions. (These constants are listed in Ref. 25).

The following values are assigned to the remaining model parameters: $k_6 = 2.9\ \mathrm{s}^{-1}$, $g = 0.42$, $k_0 =$ flow rate/reactor volume $= 7.8\times10^{-3}\mathrm{s}^{-1}$, and $A_0 =$ feed concentration of $BrO_3^- = 0.14$ M. We vary Y_0 and C_0, the feed concentrations of Br^- and Ce^{3+}, respectively, as will now be discussed.

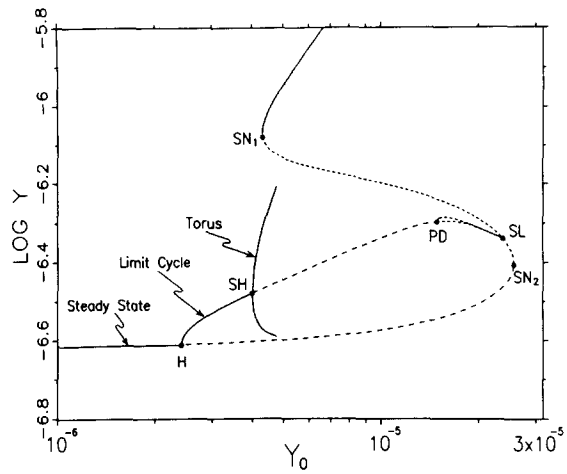

FIG. 1. Bifurcation diagram. Three kinds of states are shown: steady states, limit cycles, and tori. Solid lines denote stable states; short dashed lines, states with one unstable direction; long dashed lines, states with two unstable directions. (For steady states the number of unstable directions is the number of eigenvalues with positive real part; for limit cycles the number of unstable directions is the number of Floquet multipliers outside the unit circle.) H denotes Hopf bifurcation ($Y_0 = 2.419\times10^{-6}$ M), SH denotes secondary Hopf bifurcation ($Y_0 = 4.007\times10^{-6}$ M), SN_1 and SN_2 denote saddle-node bifurcations ($Y_0 = 4.300\times10^{-6}$ M and $Y_0 = 2.574\times10^{-5}$ M, respectively), PD denotes period-doubling bifurcation ($Y_0 = 1.494\times10^{-5}$ M), SL denotes saddle-loop bifurcation ($Y_0 \simeq 2.38\times10^{-5}$ M),

III. RESULTS

A. Variation of Y_0

We first describe a sequence of transitions which takes place as Y_0 is varied (C_0 fixed at 1.25×10^{-4} M). The states of the system as a function of Y_0 are summarized in the bifurcation diagram shown in Fig. 1. Three kinds of states are shown: fixed points (steady states), limit cycles (periodic oscillations), and tori (quasiperiodic oscillations). For the steady states the value of log Y is plotted, with dashed lines used to indicate unstable states. For the limit cycles the maximum value of log Y on the orbit is plotted, and again dashed lines are used to indicate unstable states. For the torus, the amplitude of the oscillations varies [see Figs. 2(b) and 2(c) discussed below], so we plot the maximum and minimum values of the upper envelope of the oscillations. The steady state and limit cycle branches were computed using continuation methods[37–39] and the torus branch was obtained by direct numerical integration (Gear method).[40]

We describe the bifurcation diagram from left to right. For low values of Y_0 there exists only a single stable steady state and at the point labeled H this steady state becomes unstable to oscillations via a Hopf bifurcation. Figure 2(a) shows the periodic oscillations obtained just above this bifurcation. At the point labeled SH there is a secondary Hopf or Naimark–Sacker torus bifurcation (see below) and this limit cycle becomes unstable to a quasiperiodic (two frequency) state in much the same way as the steady state became unstable to oscillations at the Hopf bifurcation. Figure 2(b) shows the quasiperiodic oscillations obtained just above the secondary Hopf bifurcation.

To verify the transition to quasiperiodicity we have computed the characteristic, or Floquet, multipliers of the

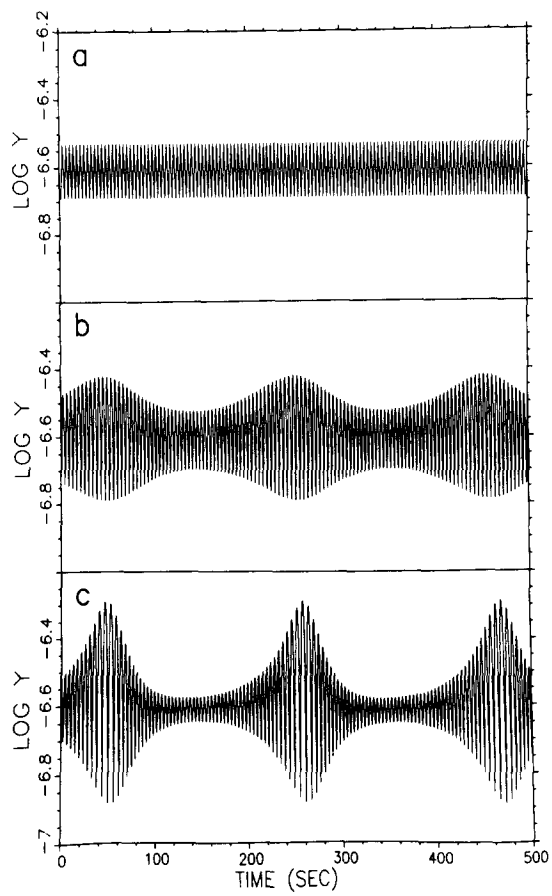

FIG. 2. Time series for three values of Y_0 showing the evolution of oscillatory behavior. (a) $Y_0 = 3.0\times10^{-6}$ M, (b) $Y_0 = 4.05\times10^{-6}$ M, (c) $Y_0 = 4.4\times10^{-6}$ M.

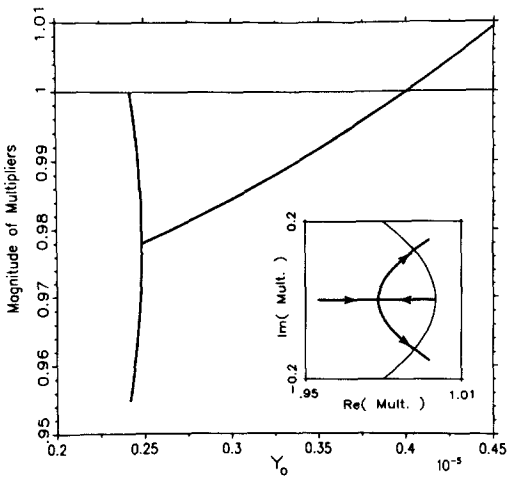

FIG. 3. The evolution with Y_0 of the magnitude of the two largest Floquet multipliers of the periodic orbit. The inset shows the real and imaginary parts of these multipliers, with arrows indicating the direction of increasing Y_0 (because of the choice of scales, the unit "circle" is elliptical). The multipliers cross the unit circle transversally at $Y_0 = 4.007 \times 10^{-6}$ M.

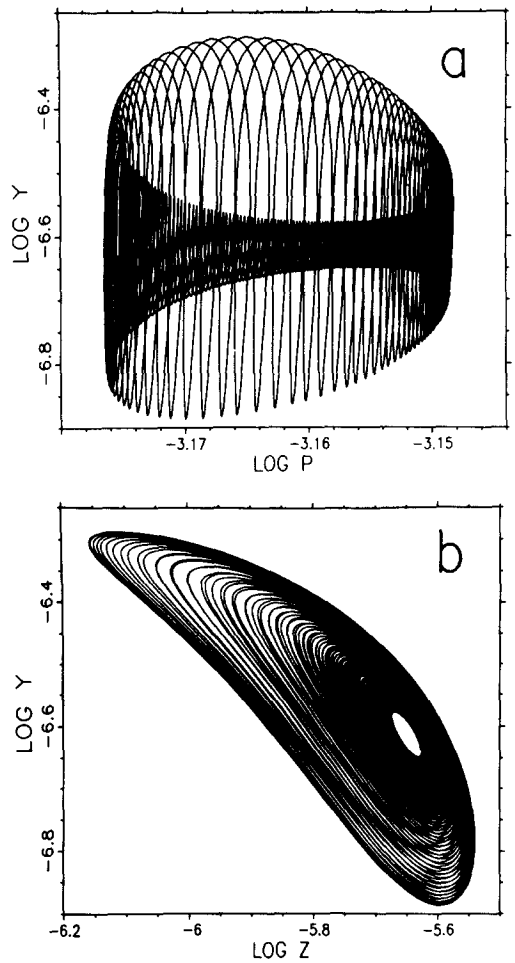

FIG. 4. Two projections of the phase portrait corresponding to the time series of Fig. 2(c) ($Y_0 = 4.4 \times 10^{-6}$ M).

periodic orbit. These multipliers give stability information about the limit cycle in the same way that eigenvalues give stability information about fixed points; multipliers outside the unit circle (in the complex plane) are associated with unstable directions for the limit cycle. The behavior of the two multipliers of largest magnitude, from the orbit's birth through the quasiperiodic transition, is shown in Fig. 3. As Y_0 is increased through the transtion value ($Y_0 = 4.007 \times 10^{-6}$ M), a complex conjugate pair of multipliers is seen to pass transversally through unit magnitude (at $0.992 \pm 0.126i$). This verifies that the limit cycle loses stability to quasiperiodicity via a secondary Hopf or Naimark–Sacker torus bifurcation (see Ref. 15).

Beyond the secondary Hopf bifurcation, the amplitude of the second mode increases rapidly with increasing Y_0. Figure 2(c) shows a time series when the second mode has become quite large and Fig. 4 shows two projections of the phase portrait of these quasiperiodic oscillations. The toroidal geometry is clearly seen in Fig. 4.

At the point labeled SN_1 there is a saddle-node bifurcation giving rise to a pair of fixed points, one stable and one unstable. The unstable steady state coalesces with the original steady state in a saddle-node bifurcation at SN_2, thereby giving the S-shaped steady state curve. The stable steady state exists for arbitrarily large values of Y_0.

From Fig. 1 it is evident that the region of quasiperiodic behavior extends past the saddle-node bifurcation at SN_1; thus there is a region of bistability between the torus and the stable steady state created at SN_1. For some value of Y_0 between 4.74×10^{-6} and 4.78×10^{-6} M, the torus becomes unstable or ceases to exist, and for all larger values of Y_0 the only attractor is the stable steady state. Investigations of the basins of attraction for the torus and upper steady state indicate that the torus is destroyed by colliding with an unstable torus (saddle-node-of-tori bifurcation). Our inability to compute unstable tori prevents the direct confirmation of this, however.

The remaining feature of Fig. 1 which we wish to discuss is the termination of the limit cycle as Y_0 is increased, for this will be of importance in a comparison with normal forms. The limit cycle terminates in a saddle-loop bifurcation (homoclinic orbit) of the fixed point on the middle branch of the steady state curve; however, there is a complication. Before the limit cycle terminates, it undergoes a period-doubling bifurcation at the point labeled PD. The period-doubled orbit undergoes a period-doubling bifurcation (not shown) to a period-four state at $Y_0 = 1.521 \times 10^{-5}$. We have not investigated the period-four state, but it is quite possible that a full period-doubling cascade follows.

As the saddle-loop bifurcation is approached, the period-doubled limit cycle approaches the primary limit cycle and the periods of both tend to infinity. Due to the additional involvement of the period-doubled orbits, the situation is quite complex at the termination of the original limit cycle.

B. Variation of C_0

In this section we describe the transitions observed as C_0 is varied (Y_0 fixed at 4.2×10^{-6} M). Again the states of the system as a function of C_0 are conveniently summarized in a bifurcation diagram: Fig. 5. In addition to the states appearing on the previous bifurcation diagram, we have here a state

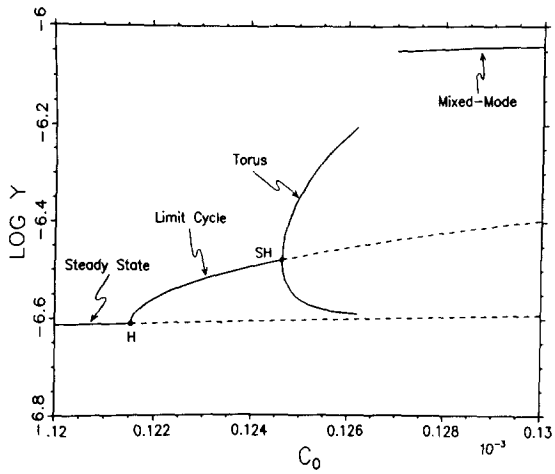

FIG. 5. Bifurcation diagram. Four kinds of states are shown: steady states, limit cycles, tori, and mixed-mode oscillations. Solid lines denote stable states; dashed lines, states with two unstable directions. H denotes Hopf bifurcation ($C_0 = 1.215\times10^{-4}$ M), SH denotes secondary Hopf bifurcation ($C_0 = 1.246\times10^{-4}$ M).

which we call mixed-mode oscillations. Such oscillations exhibit both relaxational and nearly harmonic phases [see Figs. 6(c) and 7 discussed below]. For these states the maximum value of log Y of the oscillations is plotted. Though there must exist stable oscillatory states between the quasiperiodic and mixed-mode oscillations, these are not indicated in Fig. 5 because numerical integration gives unreliable results for these oscillations (see below). Only a portion of the behavior found by varying C_0 is shown—that containing the transition from steady state to mixed-mode oscillations.

We first describe the gross features of the C_0 bifurcation diagram, then discuss the detailed structure we have observed. There exists only a single steady state over the range of C_0 values shown, although there does exist bistability at lower values of C_0. For low values of C_0 the steady state is stable and, as before, it loses stability to oscillations via a Hopf bifurcation. A periodic state obtained just above the Hopf bifurcation is shown in Fig. 6(a). Again, the periodic oscillations become unstable to quasiperiodic oscillations via a secondary Hopf bifurcation. Figure 6(b) shows such oscillations after the second mode has become quite large. There is then a transition, which we have yet to characterize, between the quasiperiodic oscillations and the mixed-mode oscillations shown in Fig. 6(c). [The time scale of Fig. 6(c)

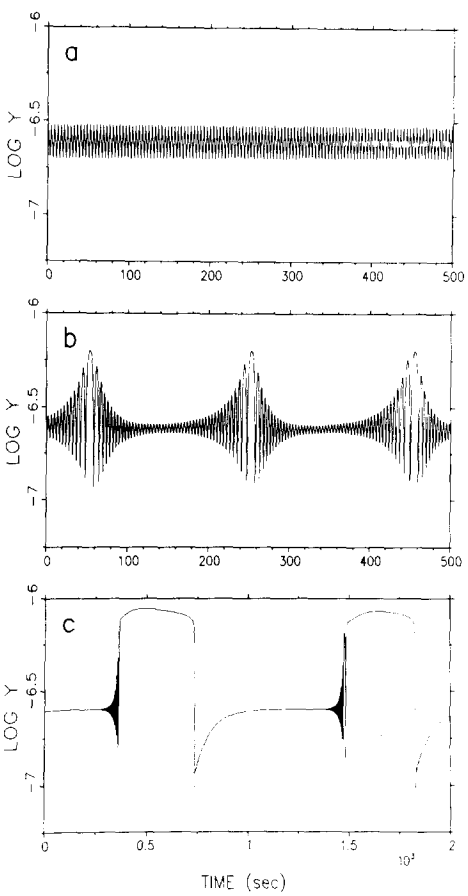

FIG. 6. Time series for three values of C_0 showing the evolution of oscillatory behavior. (a) $C_0 = 1.23\times10^{-4}$ M, (b) $C_0 = 1.2625\times10^{-4}$ M, (c) $C_0 = 1.27\times10^{-4}$ M.

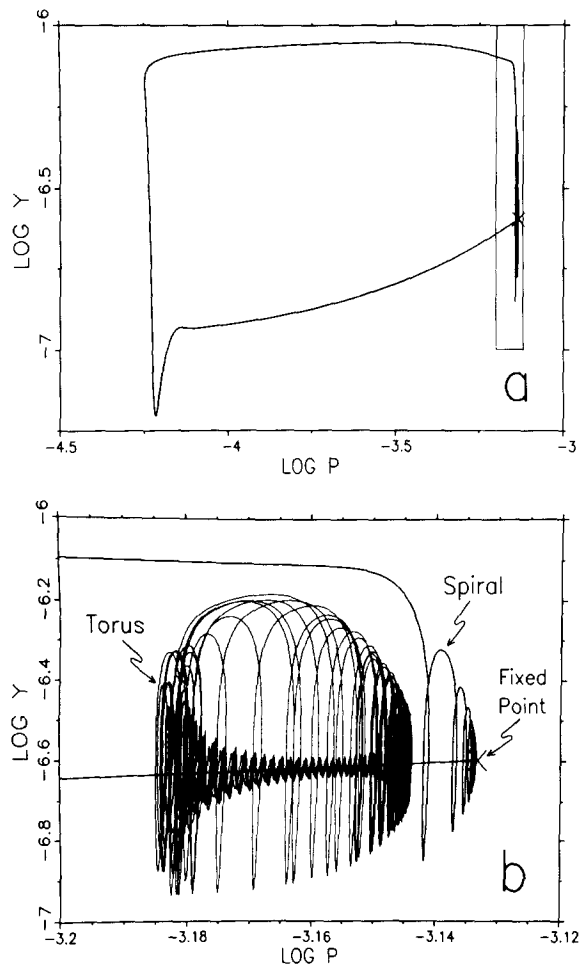

FIG. 7. Phase portraits showing the geometrical relationship between the torus associated with quasiperiodic oscillations and the spiral attractor associated with mixed-mode oscillations. (a) Part of the spiral attractor and the saddle-focus fixed point at $C_0 = 1.27\times10^{-4}$ M. Only one large excursion is shown. (b) Enlargement of the boxed region in (a) together with the torus of Fig. 6(b). Note that the spiral and fixed point are for $C_0 = 1.27\times10^{-4}$ M; the torus is for $C_0 = 1.2625\times10^{-4}$ M.

is such that the individual nearly harmonic oscillations are not visible. These oscillations are visible, however, in the phase portrait of Fig. 7(b).] Thus we observe that between the small amplitude oscillations arising from the Hopf bifurcation and the mixed-mode oscillations, there is a secondary Hopf bifurcation and quasiperiodicity.

Our inability to characterize the transition between the quasiperiodic and mixed-mode oscillations is largely due to the failure of numerical methods in the transition region. For values of C_0 between 1.2625×10^{-4} M and approximately 1.27×10^{-4} M, the solutions obtained by numerical integration fail to converge; the qualitative character of the solutions changes as the precision of the numerical integration is increased. Even when the single-step error is reduced to less than 1 part in 10^{14} we obtain no convergence of results. Thus in the transition region we cannot reliably determine even the qualitative behavior of the model.

Nevertheless, there is a geometrical relationship between the torus and the mixed-mode oscillations. This is evident in the phase portraits of Fig. 7. Figure 7(a) shows the first 1200 s of the data of Fig. 6(c) together with the fixed point at the same value of C_0. The spiral attractor corresponding to the mixed-mode oscillations is referred to as a Silnikov spiral[41]; the fixed point is called a saddle focus (it has a complex conjugate pair of eigenvalues with positive real part and three eigenvalues which are real and negative). Figure 7(b) shows an enlargement of the boxed region of Fig. 7(a) together with the torus of Fig. 6(b), thereby revealing the relationship between the mixed-mode oscillations and the torus. The enlargement of the spiral in Fig. 7(b) also makes clear the way trajectories on this attractor closely approach the saddle-focus fixed point before spiralling away (in nearly harmonic oscillations) to make large excursion (relaxation oscillation) seen in Fig. 7(a).

While trajectories almost always make the full excursion shown in Fig. 7(a), they are observed occasionally to make a smaller excursion before returning to the vicinity of the fixed point. We are as yet unable to determine whether these small excursions are real or an artifact of numerical noise.

Having described the coarse features of the bifurcation diagram, we now discuss some transitions we have observed by looking carefully between the secondary Hopf bifurcation and the transition to the mixed-mode oscillations. The observed states are summarized in the six Poincaré sections of Fig. 8. Figure 8(a) shows a section of the smooth torus as it exists just past the secondary Hopf bifurcation. Figure 8(b) shows that at a slightly larger value of C_0, trajectories are phase-locked on the torus; the oscillations are periodic with 49 oscillations per period (rotation number = 1/49). Increasing values of C_0 give at least two period doublings (not shown) from this periodic state, and while it is possible that a

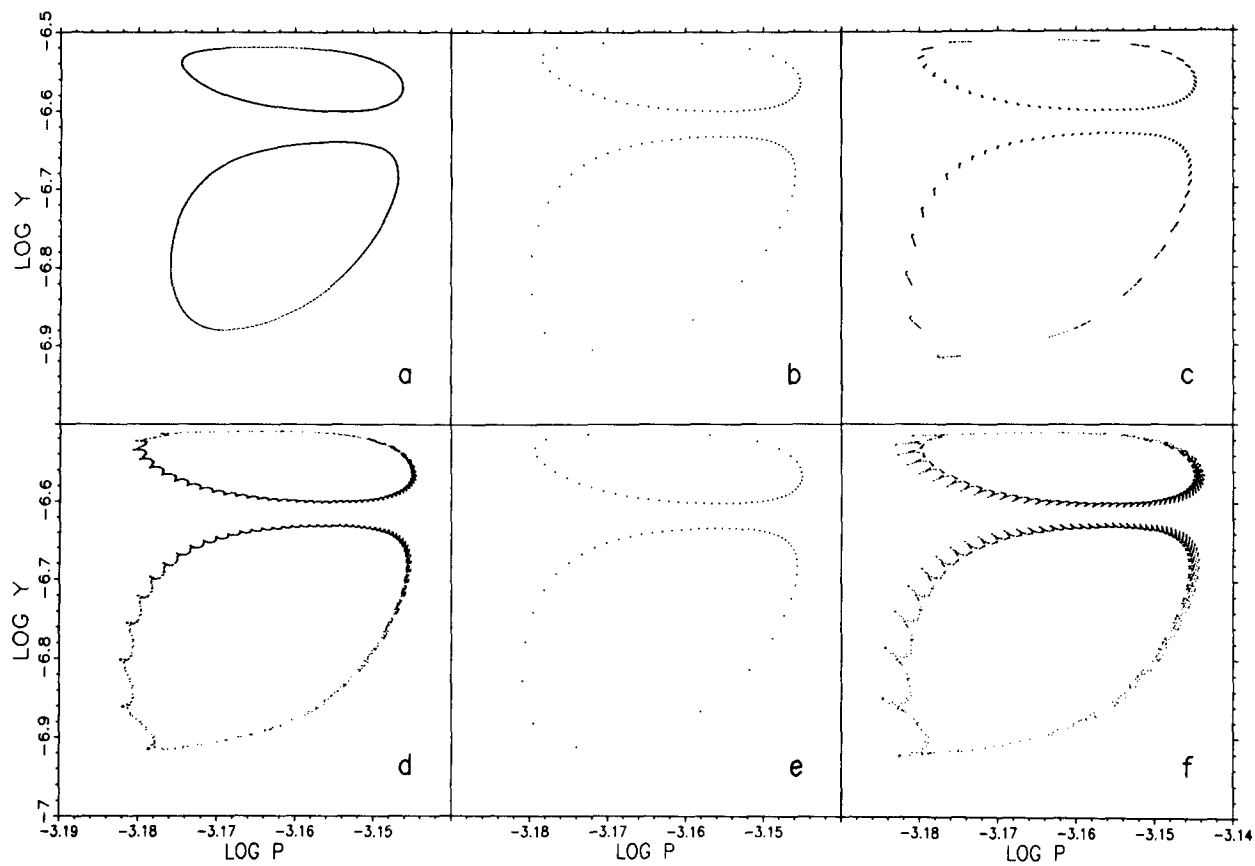

FIG. 8. Projections of six Poincaré sections (section surface: $Z = 2.288\times10^{-6}$ M). (a) $C_0 = 1.255\times10^{-4}$ M, smooth torus, (b) $C_0 = 1.26\times10^{-4}$ M, phase locking on torus (rotation number 1/49), (c) $C_0 = 1.261\,21\times10^{-4}$ M, bands on wrinkled torus, (d) $C_0 = 1.2615\times10^{-4}$ M, wrinkled torus, (e) $C_0 = 1.2618\times10^{-4}$ M, phase locking on torus (rotation number 1/48), (f) $C_0 = 1.2625\times10^{-4}$ M, wrinkled torus.

full period-doubling cascade follows, no attempt has been made to locate states of very high period.

Beyond the region of period doubling we have observed, with increasing C_0, bands on a wrinkled torus [Fig. 8(c)], then a more uniformly filled out wrinkled torus [Fig. 8(d)], followed again by phase locking, now with rotation number 1/48 [Fig. 8(e)]. Following this phase-locked state we have again found period-doubled states (not shown), bands on a wrinkled torus (not shown either), and finally the very wrinkled torus shown in Fig. 8(f). The torus of Fig. 8(f) is the same state as shown in Figs. 6(b) and 7(b), and is the last state observed before the region in which numerical methods fail.

IV. DISCUSSION

We now examine how the results of our model studies are related to other studies of the BZ reaction. We shall emphasize the significance of our results to experimental observations of quasiperiodicity and to the interpretation of these observations in terms of the hysteresis–Hopf bifurcation. We therefore begin with a brief discussion of the hysteresis–Hopf bifurcation and a summary of pertinent results obtained from the corresponding normal form.

A. The hysteresis–Hopf normal form

The dynamics that exists near (in parameter space) a hysteresis–Hopf bifurcation is governed by the hysteresis–Hopf normal form (HHNF). The normal form equations, as given by Langford,[14,15] are

$$\begin{aligned} \dot{x} &= x(z-\beta) - \omega y, \\ \dot{y} &= \omega x + y(z-\beta), \\ \dot{z} &= \lambda + \alpha z - z^3/3 - (x^2+y^2)b, \end{aligned} \tag{1}$$

where α, β, and λ are parameters, and ω and b are nonzero constants. This normal form is a simple system of equations, having a hysteresis–Hopf bifurcation (at $\alpha=\beta=\lambda=0$), which serves as an archetype for systems exhibiting this bifurcation.[42] (For a general discussion of normal forms, see Ref. 43.)

We begin by giving the conditions under which the above normal form possesses Hopf and hysteresis bifurcations and describe the way these come together in a hysteresis–Hopf bifurcation. The steady states of Eqs. (1) are easily found to be $x_{ss}=y_{ss}=0$ and z_{ss} a solution of

$$0 = \lambda + \alpha z_{ss} - z_{ss}^3/3$$

and the Jacobian of Eqs. (1) evaluated at steady state is found to be

$$\begin{bmatrix} z_{ss}-\beta & -\omega & 0 \\ \omega & z_{ss}-\beta & 0 \\ 0 & 0 & \alpha - z_{ss}^2 \end{bmatrix}. \tag{2}$$

We first discuss the hysteresis bifurcation. For $\alpha<0$ there is a single value of z_{ss} for each value of λ. Correspondingly, the Jacobian has no zero eigenvalues when $\alpha<0$. For $\alpha>0$ there are two saddle-node bifurcations (at $\lambda=\pm\frac{2}{3}\alpha^{3/2}$) and three steady states for each value of λ between these bifurcations. The saddle nodes correspond to points where the Jacobian has a zero eigenvalue ($z_{ss}=\pm\alpha^{1/2}$). At $\alpha=0$, the saddle nodes come together (at $\lambda=0$) and we have a hysteresis point or hysteresis bifurcation. This is shown in Fig. 9(a). At the hysteresis point, the Jacobian still has a zero eigenvalue; however, it is no longer a simple zero, for $\partial^2\dot{z}/\partial z^2=0$ at $\alpha=\lambda=0$. This violates one of the conditions needed to guarantee a saddle-node bifurcation[43] and, as a result, we have the more degenerate hysteresis bifurcation.

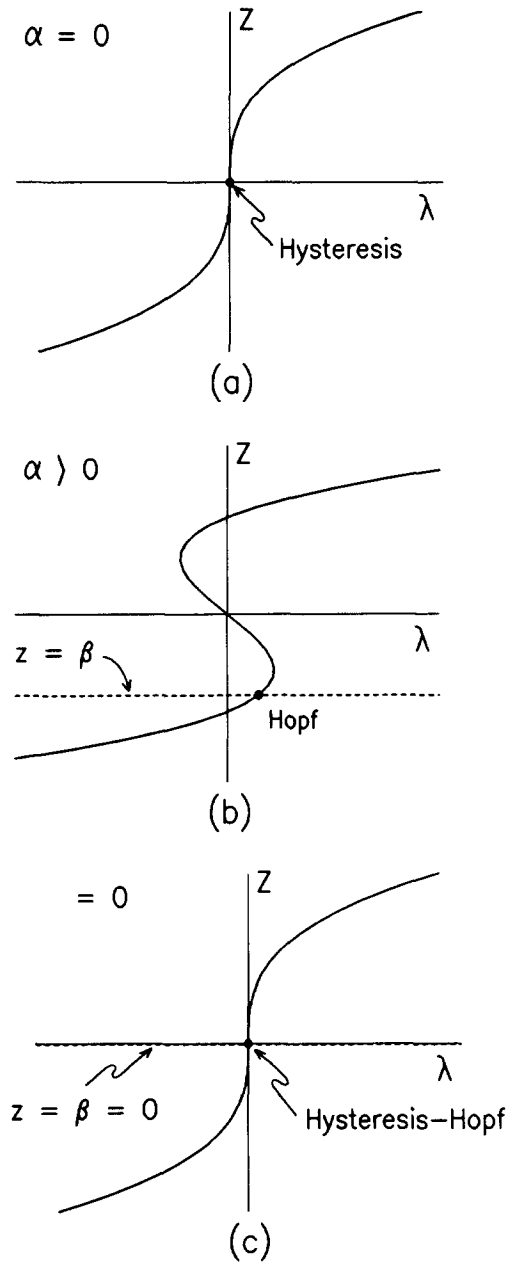

FIG. 9. Plots of z_{ss} as a function of λ for different parameter values in the hysteresis–Hopf normal form. (a) $\alpha=0$: a hysteresis bifurcation at $\lambda=0$. (b) $\alpha>0$ and $\beta<0$: the intersection of the line $z=\beta$ with steady state curve showing the occurrence of a Hopf bifurcation. (c) $\alpha=\beta=0$: the coalescence of hysteresis and Hopf bifurcations in a hysteresis–Hopf bifurcation at $\lambda=0$.

A Hopf bifurcation occurs when a complex conjugate pair of eigenvalues (of the Jacobian evaluated at steady state) crosses the imaginary axis. We see from the above

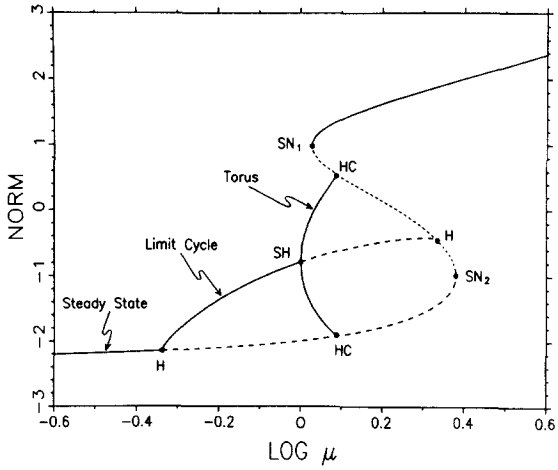

FIG. 10. Bifurcation diagram for the hysteresis–Hopf normal form. Three kinds of states are shown: steady states, limit cycles, and tori. Solid lines denote stable states; long dashed, states with two unstable directions; short dashed, states with one unstable direction; very short dashed (between H and SN_2), states with three unstable directions. H denotes Hopf bifurcation, SH denotes secondary Hopf bifurcation, SN_1, and SN_2 denote saddle-node bifurcations, HC denotes heteroclinic connection.

Jacobian that this occurs in the normal form when $\beta = z_{ss}$. Figure 9(b) shows a Hopf bifurcation on the steady state curve for the case $\alpha > 0$ and $\beta < 0$.

When $\alpha = \beta = \lambda = 0$, the Hopf and hysteresis bifurcations coalesce at $x_{ss} = y_{ss} = z_{ss} = 0$ and we have a steady state with a zero and a pure imaginary pair of eigenvalues. These eigenvalues, together with the hysteresis degeneracy, define the hysteresis–Hopf bifurcation [see Fig 9(c)].

We now turn to the dynamics generated by the hysteresis–Hopf normal form, for this is the dynamics that we can expect to find near a hysteresis–Hopf bifurcation. Because Hopf and hysteresis bifurcations exist separately near the hysteresis–Hopf bifurcation, we know that there exist both oscillations and multiple steady states arbitrarily close to this point; moreover, due to nonlinear interaction, other more complicated dynamics can also exist near a hysteresis–Hopf bifurcation. In particular it has been shown that tori exist near such a bifurcation.[14]

Figure 10 shows a bifurcation diagram generated from the normal form. As on previous bifurcation diagrams, steady states, limit cycles, and tori are shown. The parameter path shown in Fig. 10 is different than that chosen for discussion elsewhere.[15,22,23] In particular, Fig. 10 corresponds to a "curved" path in the parameter space (α,β,λ) given parametrically by $\alpha = 1$, $\beta = 1/\mu$, $\lambda = 1.73 - \mu$, with μ the bifurcation parameter. In is necessary to take such a curved path to achieve a bifurcation diagram with a bounded region of oscillatory behavior. (Bifurcation diagrams shown elsewhere have λ as the bifurcation parameter and have an unbounded region of oscillatory behavior). The norm used to represent each of the states in Fig. 10 is like that used on the previous bifurcation diagrams.

The bifurcation diagram shown in Fig. 10 can be described briefly as follows. At low values of μ there is a stable steady state which gives rise to oscillations via Hopf bifurcation. These oscillations in turn give rise to quasiperiodicity via secondary Hopf bifurcation. There is then a saddle-node bifurcation (labeled SN_1) from which a pair of steady states emerges, one stable and one unstable. This leads to bistability between the torus and the stable steady state created at SN_1. At the points labeled HC, the torus forms a heteroclinic connection with the middle and lower fixed points and at this point the torus is destroyed (see Ref. 15). At this heteroclinic connection the diameter of the hole of the torus has shrunk to zero. Beyond this bifurcation the unstable limit cycle terminates in a Hopf bifurcation on the middle branch of the steady state curve. The middle and lower fixed points then come together in a saddle-node bifurcation at the point labeled SN_2, thereby completing the S-shaped steady state curve.

We note that the heteroclinic connection destroying the torus can occur in two other ways, resulting in two other bifurcation diagrams slightly different from that shown in Fig. 10. In the first of these, the heteroclinic connection destroying the torus occurs simultaneously with the upper saddle-node bifurcation. Then there is no bistability between the torus and the upper steady state. (This is as in the bifurcation diagrams shown in Refs. 15, 22, and 23.) In the other case, the heteroclinic connection produces an unstable torus rather than destroying the stable one. The unstable torus and the stable torus then collide in a saddle-node-of-tori bifurcation and both are destroyed. The effective difference between the bifurcation diagram associated with this last case and that of Fig. 10 is that the stable torus loses stability without the diameter of the hole of the torus shrinking to zero.

B. Comparison of model with experiment and the hysteresis–Hopf normal form

We now compare the model results first described (Y_0 varied) with experimental results obtained by Argoul and Roux[12] and with the bifurcation diagram for the HHNF discussed in the preceding subsection. For convenience we make the following definition: an *observable scenario* in a dynamical system is a sequence of attracting dynamical states obtained through the variation of an external parameter. (We include the possibility of more than one attracting state at points along the parameter path.) Thus an observable scenario is a scenario that can be seen either through experiment or through direct numerical integration of a system of differential equations. With this definition we note that the observable scenario found in each of the three cases, model, experiment, and HHNF, is essentially the same. This means, in particular, that the observable scenario reported by Argoul and Roux can be found in the vicinity of a hysteresis–Hopf bifurcation. This, together with the ubiquity of hysteresis and Hopf bifurcations in the BZ reaction, has led to the interpretation of these results in terms of the hysteresis–Hopf bifurcation.[12,22,23] This is certainly a plausible explanation for their experimental results; however, we have found essentially the same observable scenario in our model studies and yet we can show that when all the dynamics along the parameter path is considered, the hysteresis–Hopf normal form cannot account for the model behavior. We now elaborate.

In the experiments, flow rate was used as the bifurcation parameter. A transition from periodic to quasiperiodic oscillations via a secondary Hopf bifurcation was observed as the flow rate, was increased. The amplitude of the second mode was found to grow very rapidly with further increases in flow rate, and the hole of the torus shrank to a thin tube. The torus did not exist for larger values of flow rate and instead a marginally stable steady state was observed.

While the experimental observations are very similar to those we have reported in our model simulations, there are slight difference in the two cases. (1) While in the model simulations the hole of the torus was found to shrink very rapidly with increasing Y_0, it did not shrink completely as in the experimental case. (2) We found bistability between the torus and the upper steady state in the model simulations. No such bistability was reported in the experimental results, though it might have existed over a range too small to be observable.

The differences between the *model* and *experiment* can be attributed to differences in the heteroclinic connection which results in the destruction of the torus. The variants of this bifurcation were discussed in the context of the HHNF at the end of the preceding subsection. In the experiment, the heteroclinic connection and the saddle-node bifurcation occur simultaneously—thus the absence of bistability. In the model, the heteroclinic connection produces an unstable torus which then collides with the stable torus. This causes the stable torus to lose stability with a finite-diameter hole. We consider these differences between model and experiment minor and probably removable with changes in other parameters.

We remark that we have not made an attempt to match the parameter values in our study with those of experiment. In particular, we have used Y_0 as a bifurcation parameter rather than flow rate. While it is possible to vary flow rate in the model and produce a torus through a secondary Hopf bifurcation, we did not find such a parameter path which would allow for clear comparison with HHNF. Because it is the interpretation of the quasiperiodic dynamics in terms of the hysteresis–Hopf bifurcation which interests us here, we report the Y_0 bifurcation diagram.

Having noted the resemblance of the model and experimental results, we now compare the model behavior with the normal form HHNF. From our previous discussions of the model results and the HHNF it is clear that *identical observable scenarios* can be found in the model and normal form. Despite this, there is a conflict between the HHNF and the model which centers around the termination of the limit cycle after the secondary Hopf bifurcation.

In the HHNF, the unstable limit cycle terminates in a Hopf bifurcation on the middle branch of the steady state curve (see Fig. 10), whereas in the model studies this limit cycle terminates (after undergoing a period-doubling bifurcation) in a saddle-loop bifurcation of the middle fixed point. Because the saddle-loop bifurcation does not involve any change in the stability of the middle fixed point (i.e., in the number of positive eigenvalues), the fixed point has one positive eigenvalue along the entire middle branch. This is in contrast with the HHNF, wherein the number of eigenvalues with positive real part on the middle branch changes from one to three at the Hopf bifurcation. The saddle-node SN_2 (Fig. 1) in the model is thus a point of coalescence of a steady state with one positive eigenvalue and a steady state with two positive eigenvalues, and so has a single positive eigenvalue (along with the requisite zero eigenvalue and the three negative ones). Note, however, that at a saddle-node bifurcation in the HHNF, the two nonzero eigenvalues of the Jacobian matrix (2) are of the form $(z_{ss} - \beta) \pm i\omega$, where $\omega \neq 0$. Thus, saddle nodes in the HHNF can have either two eigenvalues with positive real part ($z_{ss} > \beta$), or none ($z_{ss} \leqslant \beta$), but not a single positive real eigenvalue as in the model.

From this we conclude that the HHNF is incapable of giving the model behavior, and that, if a single normal form is to account for the dynamics of the SNB model, then it must exhibit a saddle node with a single positive real eigenvalue. The only normal forms showing this feature are those having a linearization with at least two zero eigenvalues.

We make a final note concerning the relationship between the model and the HHNF. In an effort to find in the model the same behavior as is in the normal form, we have made systematic attempts to locate a Hopf bifurcation of the middle branch of the steady state surface.[37] All such attempts have failed.

C. Relevance of model results to other features of the BZ reaction

We now reexamine the results obtained from the model by varying the parameter C_0 with regard to the relationship of the torus to other features of the BZ reaction. We begin with the transition from small amplitude to mixed mode oscillations. This transition was observed in some of the earliest experiments on the BZ reaction in flow reactors,[1,2] but has yet to be fully understood. While there may be more than one way to achieve this transition, our simulations show that it can be mediated by a secondary Hopf bifurcation and hence by quasiperiodicity.

The gauge whether this intermediacy of quasiperiodicity is unusual or common in the model, we looked elsewhere in the model at the transition from small to mixed-mode oscillation and again a torus was found.[44] The parameter range over which these tori were seen to exist is quite small. However, this may not be the case everywhere and more importantly, since we expect only qualitatively reliable results from the model simulations,[32] the corresponding parameter range in laboratory experiments may be larger or smaller. We suggest that well-controlled experiments and numerical studies of other models of this reaction might also reveal tori between small amplitude and mixed-mode oscillations. A more detailed treatment of this transition in terms of bifurcation theory will be presented elsewhere.

We now turn to the feature of the BZ reaction which has received the most attention in recent years—sequences of alternating periodic and chaotic states in which the number of oscillations per period of consecutive periodic states differs by one.[2,3,5,9,13,22,23,36,45] Although we have not computed Lyapunov exponents for the wrinkled tori of Figs.

8(c), 8(d), and 8(f), the stretching and folding associated with chaotic dynamics is apparent in these attractors. (States such as these are commonly seen to arise from smooth tori.[16–23]) Note that because there is one more oscillation per period in the state shown in Fig. 8(b) than in the state shown in Fig. 8(e), Fig. 8 shows a limited periodic–chaotic sequence evolving from a smooth torus. This provides a clear connection between this particular periodic–chaotic sequence and phase locking and unlocking on a wrinkled torus. It is possible that this interpretation is valid for other periodic–chaotic sequences seen in the BZ system but that the underlying torus is not as apparent as in this case.

V. CONCLUSION

We have presented the first observation of quasiperiodicity in a model of the BZ reaction and have described the evolution of the associated torus along two paths in the parameter space of the model. We have noted the resemblance of the model simulations to experimental observations and to the dynamics found in the vicinity of a hysteresis–Hopf bifurcation. We have shown that while the interaction of Hopf and hysteresis bifurcations can give rise to dynamics similar to that seen in the model, it is not possible to interpret the model behavior simply in terms of the hysteresis–Hopf normal form.

These results suggest that the dynamics underlying the quasiperiodicity seen experimentally might also be more complex than previously thought. If the Oregonator model which we have studied provides a true qualitative description of the dynamics of the BZ reaction, then a normal form other than that of the hysteresis–Hopf bifurcation will be necessary for a proper interpretation of the dynamics of the reaction.

We have found that the transition from small amplitude to mixed-mode oscillations can be mediated by a secondary Hopf bifurcation and quasiperiodicity and that this mediation may be common in the model. This suggests that tori might be found experimentally in the transition region. Finally, we have shown that the model possesses a sequence of periodic and chaotic states and that this sequence arises from the phase locking and unlocking on a wrinkled torus.

ACKNOWLEGEMENTS

We wish to thank David Lindberg for suggesting a potentially fruitful region of parameter space. This work has been supported in part by a grant from the Robert A. Welch Foundation (F-914).

[1]R. A. Schmitz, K. R. Graziani, and J. L. Hudson, J. Chem. Phys. **67**, 3040 (1977).
[2]J. L. Hudson, M. Hart, and D. Marinko, J. Chem. Phys. **71**, 1601 (1979).
[3]J. L. Hudson and J. C. Mankin, J. Chem. Phys. **74**, 6171 (1981).
[4]J. C. Roux, A. Rossi, S. Bachelart, and C. Vidal, Phys. Lett. A **77**, 391 (1980).
[5]J. S. Turner, J.-C. Roux, W. D. McCormick, and H. L. Swinney, Phys. Lett. A **85**, 9 (1981).
[6]J. C. Roux, R. H. Simoyi, and H. L. Swinney, Physica D **8**, 257 (1983).
[7]J. Ringland and J. S. Turner, Phys. Lett. A **105**, 93 (1984).
[8]M. Hourai, Y. Kotake, and K. Kuwata, J. Phys. Chem. **89**, 1760 (1985).
[9]P. Richetti and A. Arneodo, Phys. Lett. A **109**, 359 (1985).
[10]J. Maselko and H. L. Swinney, J. Chem. Phys. **85**, 6430 (1986).
[11]J. C. Roux and A. Rossi, in *Non-Equilibrium Dynamics in Chemical Systems*, edited by C. Vidal and A. Pacault (Springer, New York, 1984), p. 141.
[12]F. Argoul and J. C. Roux, Phys. Lett. A **108**, 426 (1985).
[13]F. Argoul, A. Arneodo, P. Richetti, and J. C. Roux, J. Chem. Phys. **86**, 3325 (1987).
[14]W. F. Langford, SIAM J. Appl. Math. **37**, 22 (1979).
[15]W. F. Langford, in *Nonlinear Dynamics and Turbulence*, edited by G. I. Barenblatt, G. Iooss, and D. D. Joseph (Pitman, Boston, 1982), p. 215.
[16]J. H. Curry and J. A. Yorke, in *Lecture Notes in Mathematics*, edited by A. Dold and B. Eckmann (Springer, New York, 1978), Vol. 668, p. 48.
[17]D. G. Aronson, M. A. Chory, G. R. Hall, and R. P. McGehee, Commun. Math. Phys. **83**, 303 (1982).
[18]M. R. Guevara and L. Glass, J. Math. Biol. **14**, 1 (1982).
[19]V. Franceschini, Physica D **6**, 285 (1983).
[20]W. F. Langford, in *International Series of Numerical Mathematics*, edited by T. Kupper, H. D. Mittelmann, and H. Weber (Birkhauser, Basel, 1984), Vol. 70, p. 285.
[21]M. J. Feigenbaum, L. P. Kadanoff, and S. J. Shenker, Physica D **5**, 370 (1982).
[22]J. C. Roux, P. Richetti, A. Arneodo, and F. Argoul, J. Mec. Th. Appl. Numéro Spécial, 77 (1984).
[23]P. Richetti, J. C. Roux, F. Argoul, and A. Arneodo, J. Chem. Phys. **86**, 3339 (1987).
[24]I. Schreiber and M. Marek, Phys. Lett. A **91**, 263 (1982).
[25]K. Showalter, R. M. Noyes, and K. Bar-Eli, J. Chem. Phys. **69**, 2514 (1978).
[26]G. R. Gavalas, *Nonlinear Differential Equations of Chemically Reacting Systems* (Springer, New York, 1968).
[27]B. L. Clarke, J. Chem. Phys. **75**, 4970 (1981).
[28]J. J. Tyson, in *Oscillations and Traveling Waves in Chemical Systems*, edited by R. J. Field and M. Burger (Wiley, New York, 1985), p. 93, and references therein.
[29]K. Bar-Eli and J. Ronkin, J. Phys. Chem. **88**, 2844 (1984).
[30]R. J. Field and H. D. Forsterling, J. Phys. Chem. **90**, 5400 (1986).
[31]R. M. Noyes, J. Phys. Chem. **90**, 5407 (1986).
[32]J. Ringland and J. S. Turner (preprint, 1987).
[33]R. J. Field, E. Körös, and R. M. Noyes, J. Am. Chem. Soc. **94**, 8649 (1972).
[34]R. J. Field, J. Chem. Phys. **63**, 2289 (1975).
[35]P. DeKepper and K. Bar-Eli, J. Chem. Phys. **87**, 480 (1983).
[36]D. Lindberg and J. S. Turner (preprint, 1987).
[37]J. Ringland, Ph.D. thesis, University of Texas, Austin, Texas, 1986.
[38]E. Doedel, *Auto: Software for Continuation and Bifurcation Problems in Ordinary Differential Equations* (Cal. Tech., Pasadena, 1986).
[39]M. Kubíček and M. Marek, *Computational Methods in Bifurcation Theory and Dissipative Structures* (Springer, New York, 1983).
[40]IMSL *Library manual*, 7th ed. (IMSL, Houston, 1979).
[41]L. P. Šilnikov, Sov. Math. Dokl. **6**, 163 (1965).
[42]The system of Eqs. (1) is actually a truncated normal form, and while higher order terms can affect the dynamics generated by this normal form, the truncation will be of no importance for results presented here.
[43]J. Guckenheimer and P. Holmes, *Nonlinear Oscillations, Dynamical Systems and Bifurcations of Vector Fields* (Spinger, New York, 1984).
[44]The torus was found at: $k_6 = 1.0\times10^{-2}$, $g = 0.47$, $A_0 = 0.10$ M, $C_0 = 8.3\times10^{-4}$, $Y_0 = 1.0\times10^{-6}$, $k_0 = 1.223\,868\,4\times10^{-3}$, and all rate constants as used here.
[45]N. Ganapathisubramanian and R. M. Noyes, J. Chem. Phys. **76**, 1770 (1982).